Numerical Modeling and Parametric Study of Additively Manufactured Cylindrical Lattice Wick Heat Pipe

Aaron M. Scott[1] and Ezra O. McNichols[2]
NASA Glenn Research Center, Cleveland, OH 44070

An axially-symmetric, 2-dimensional, revolved COMSOL Multiphysics model is created to be used in conjunction with an additively manufactured lattice wick heat pipe prototype. The model investigates the steady state performance of the heat pipe assuming compressible laminar flow in the vapor chamber and incompressible porous media flow in the wick. The conjugate heat transfer problem is solved by heat conduction transport equations and Fourier's law. The laminar vapor flow is described by Navier-Stokes equations, and the porous media flow is solved using Darcy's law. Mesh independence is verified, and a parametric study is performed on heat input, condenser length, evaporator length and heat pipe inclination. The effects on key properties including external temperature, internal temperature, internal pressure, and thermal resistance are analyzed.

Nomenclature

α	=	Thermal expansion coefficient $(1/K)$
α_p	=	Thermal expansion coefficient for non-ideal gas $(1/K)$
C_p	=	Specific heat capacity $(J/kg \cdot K)$
D_{od}	=	Outer heat pipe diameter (mm)
ϵ	=	Porosity of the wick structure
$\boldsymbol{F}$	=	Volume force vector $(N/m\text{^}3)$
h	=	Heat transfer coefficient $(W/m\text{^}2 \cdot K)$
h_{fg}	=	Specific enthalpy (J/kg)
$\boldsymbol{I}$	=	Identity matrix
k	=	Thermal conductivity $(W/m \cdot K)$
K	=	Permeability of the wick $(m\text{^}2)$
M_n	=	Molar mass of working fluid (kg/mol)
$\boldsymbol{n}$	=	Normal unit vector
$\boldsymbol{q}$	=	Convective heat flux vector $(W/m\text{^}2)$
p	=	Pressure (Pa)
Q_{in}	=	Heat input at evaporator (W)
Q_{out}	=	Heat output from the condenser (W)
Q_{hs}	=	Heat source $(W/m\text{^}3)$
ρ	=	Density $(kg/m\text{^}3)$
$\mathbf{r}$	=	Position vector (m)
R	=	Universal gas constant $(J/mol \cdot K)$
S	=	Piola-Kirchhoff stress tensor (Pa)
$\mathbf{S}$	=	Strain-rate tensor $(1/s)$
$\boldsymbol{t}$	=	Tangential unit vector
T	=	Local absolute temperature (K)
τ	=	Viscous stress tensor (Pa)
θ	=	Heat pipe inclination $(degrees)$
$\boldsymbol{u}$	=	Velocity vector (m/s)
$\boldsymbol{u}_{trans}$	=	Translational velocity vector (m/s)

Subscripts

c	=	Condenser
$cool$	=	Coolant
e	=	Evaporator
l	=	Liquid
pm	=	Porous media
ref	=	Reference
s	=	Solid
sat	=	At saturation pressure
v	=	Vapor

Introduction

A heat pipe is a passive device that enables the efficient transport of thermal energy. A typical heat pipe is a closed system, composed of a vapor chamber and a porous wick lining the chamber walls [1]. The heat pipe is evacuated, then filled with a working fluid whose thermal characteristics are appropriate for a given set of temperature ranges.

[1] Spring Intern, LTE0, NASA Glenn Research Center, Embry-Riddle Aeronautical University
[2] Research Aerospace Engineer, LTE0, MS 5-11, NASA Glenn Research Center

The chosen fluid will propagate throughout the wick and reach an equilibrium with its vapor in the vapor chamber, meaning the overall pressure in the container will be the vapor pressure at saturation conditions [1]. A heat pipe will generally be partitioned into thirds, an evaporator section, an adiabatic section, and a condenser section. When heat is applied at the evaporator section, the working fluid evaporates from the wick creating a pressure gradient in the vapor chamber that pushes the vapor to the condenser section [1]. However, in the condenser section, heat is being removed, and the vapor is condensing back into a liquid that will be absorbed by the wick [1]. This creates a pressure gradient in the wick due to capillary forces and returns the working fluid back to the evaporator section, completing the circuit [1]. The result of this heat transfer via phase transition is a virtually isothermal, high thermal conductivity device [1].

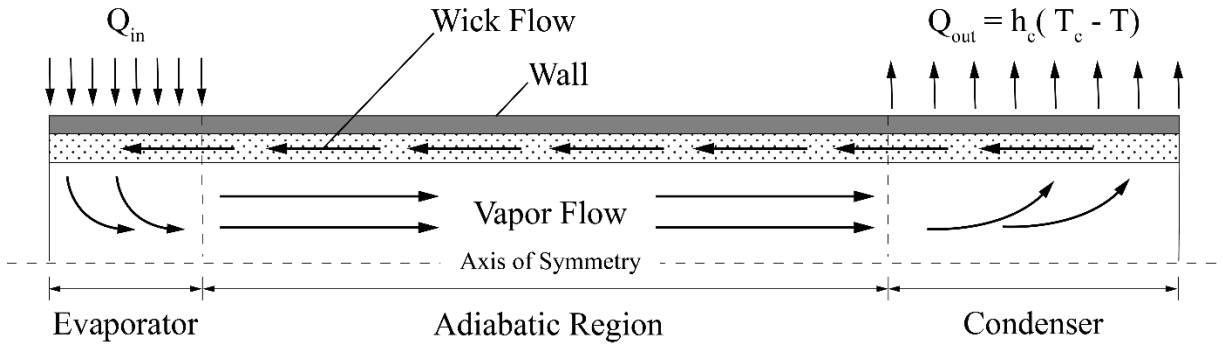

Figure 1. 2-Dimensional, halved, cross-sectional cut of the lattice wick heat pipe

The geometry of a heat pipe is somewhat arbitrary, limited primarily by manufacturing complexity. Therefore, for simplicity and generality, this paper covers the numerical modelling and simulation of an axially-symmetric, cylindrical heat pipe. The model configuration matches existing physical prototypes, made from additively manufactured Inconel 718. The configuration is parametric, allowing for variations in inclination, condenser region length, evaporator region length, and heat input. The model will be used in conjunction with real world experiments for mutual validation.

The prototype lattice wick heat pipe has an extended, smaller diameter section that is used for filling the heat pipe with the working fluid. This extended section is not included in the mathematical model.

Figure 2. Lattice wick heat pipe prototypes

I. Building the Numerical Model

Table 1. Physical Assumptions	
Domain	Assumptions
Wall Region	Uniform circumferential heating and cooling Constant heat transfer coefficient at condenser
Vapor Region	Steady state laminar flow Compressible gas flow (Mach < 0.3) Gravitational effects included Saturation pressure at inlet and outlet
Wick Region	Steady state laminar flow Incompressible Newtonian fluid flow Gravitational effects included Saturation pressure at inlet and outlet

Uniform circumferential heating and cooling are assumed at the evaporator and condenser, respectively. This allows the geometry for the numerical model to be simplified substantially, as axially-symmetric thermodynamic and fluid behavior can be assumed. This geometry is created by taking a cross-sectional cut of the cylindrical heat pipe, then cutting that cross-section in half along the axis of symmetry (See Figure 1). The simulation is performed with this halved cross-sectional cut, then the result is revolved around the axis of symmetry to generate the 3-dimensional model.

The model assumes constant material properties for the Inconel 718. The working fluid and coolant at the condenser section are both assumed to be water. See Appendix for the temperature dependent material property equations for steam and water. Table 2 contains the physical constants for the heat pipe system.

Table 2. Equation Constants		
Symbol	**Value**	**Reference**
C_{p_s}	435 $(J/kg \cdot K)$	[2]
D_{od}	6 (mm)	N/A
D_v	3.62 (mm)	N/A
ϵ	0.46	[3]
h_c	1200 $(W/m\text{^}2\ )$	[4]
h_{fg}	2.473E6 (J/kg)	[5]
K	1.305 $(m\text{^}2)$	[3]
k_s	11.4 $(w/m \cdot K)$	[2]
M_n	18.01528 (g/mol)	[5]
p_{ref}	1.0133E5 (Pa)	N/A
T_{cool}	293.15 (K)	N/A
T_{ref}	373.15 (K)	N/A

The heat pipe model is constructed in COMSOL Multiphysics 5.5. The modules used are Heat Transfer in Solids and Fluids, Laminar Flow (for flow in the vapor chamber), and Darcy's Law (for flow in the wick region). The governing equations, boundary conditions, and initial conditions are as follows:

- *For all calculations, the reference temperature,* $T_{ref} = 100°C$*, and reference pressure* $p_{ref} = 1\ atm$*.*

- *General forms of equations are provided, but steady state conditions are assumed.*
- *":" denotes a double dot product*

A. Heat Transfer

1. Governing Equations

a. In Solids

$$\rho_s C_{p_s}\left(\frac{\delta T}{\delta t}+\boldsymbol{u}_{trans}\cdot\nabla T\right)+\nabla\cdot\boldsymbol{q}_s=Q_{hs}-\alpha T:\frac{dS}{dt} \quad (1)$$

$$\boldsymbol{q}_s=-k_s\nabla T \quad (2)$$

b. In Fluids

$$\rho_v C_{p_v}\left(\frac{\delta T}{\delta t}+\boldsymbol{u_v}\cdot\nabla T\right)+\nabla\cdot\boldsymbol{q}_v=Q_{hs}+\alpha_p T\left(\frac{\delta p}{\delta t}+\boldsymbol{u_v}\cdot\nabla p_v\right)+\tau:\nabla\boldsymbol{u}_v \quad (3)$$

$$\boldsymbol{q}_v=-k_v\nabla T \quad (4)$$

$$\tau=2\mu_v\boldsymbol{S}-\frac{2}{3}\mu_v(\nabla\cdot\boldsymbol{u_v})\boldsymbol{I} \quad (5)$$

$$\boldsymbol{S}=\frac{1}{2}(\nabla\boldsymbol{u_v}+(\nabla\boldsymbol{u_v})^T) \quad (6)$$

$$\alpha_p=-\frac{1}{\rho}\frac{\delta\rho}{\delta T} \quad (7)$$

c. In Porous Media

$$\rho_l C_{p_l}\left(\frac{\delta T}{\delta t}+\boldsymbol{u}_l\cdot\nabla T\right)+\nabla\cdot\boldsymbol{q}_{pm}=Q_{hs}+\alpha_p T\left(\frac{\delta p}{\delta t}+\boldsymbol{u}_l\cdot\nabla p_l\right)+\tau:\nabla\boldsymbol{u}_l \quad (8)$$

$$\boldsymbol{q}_{pm}=-k_{eff}\nabla T \quad (9)$$

$$k_{eff}=(1-\epsilon)k_s+\epsilon k_l+k_{disp} \quad (10)$$

Variants of the heat conduction transport equation (1, 3, 8) along with Fourier's conduction law (2, 4, 9) are used to solve the conjugate heat transfer problem [6]. These equations are applied via the Heat Transfer in Solids and Fluids module. All domains are selected. Heat transfer in porous media is enabled. In equations 1, 3, and 8, the first term on the left-hand side is the heat conduction. The second term is the heat flux gradient vector. The first term on the right-hand side represents additional heat sources (when present). The second term in equation 1 accounts for thermoelastic effects in the solid [7]. The second term in equations 3 and 8 refers to the work done by pressure changes in the working fluid as a result of heating under adiabatic compression [7]. The final term on the right-hand side of equations 3 and 8 is the viscous dissipation in the fluid [7].

In fluids, equation 5 is Stokes' viscous stress tensor, which describes the stresses resulting from friction between the fluid and an element surface [8]. Equation 6 is the strain-rate tensor, which describes the rate of change of material deformation. These equations are included here to define variables used in the preceding equations, though they are not directly related to the heat transfer in the fluid. Equation 7 describes the thermal expansion coefficient for the working fluid as a function of the change in density with respect to temperature.

In porous media, equation 10 describes the volume averaged effective thermal conductivity of the wick structure, accounting for porosity, working fluid thermal conductivity, and the solid material conductivity. τ and α_p share the same definition in the porous medium domain as the fluid flow domain, except the velocity and dynamic viscosity terms refer to the liquid state of the working fluid instead of the vapor state.

2. Initial Conditions

$$T_0=293.15\ K$$

The initial temperature condition assumes that the external environmental temperature and the internal temperature of the heat pipe are in equilibrium.

3. Boundary Conditions

a. Heat Fluxes

$$\textit{Evaporator:}\quad -\boldsymbol{n}\cdot\boldsymbol{q_s} = \frac{Q_w}{\pi D_{od} L_e} \qquad (11)$$

$$\textit{Condenser:}\quad -\boldsymbol{n}\cdot\boldsymbol{q_s} = h_c(T_c - T) \qquad (12)$$

Heat fluxes are applied on the wall at the evaporator and the condenser sections. The equation at the evaporator wall represents the heat input to the system, and the equation at the condenser wall represents the heat rejection of the system. The terms on the left-hand side refer to the heat flux normal to the boundary. The term on the right-hand side of equation 11 is the applied heat flux. The term on the right-hand side of equation 12 describes the convective cooling.

b. Boundary Heat Sources

$$-\boldsymbol{n}\cdot\boldsymbol{q_v} = \rho_v h_{fg}\cdot\boldsymbol{u}_v \qquad (13)$$

Heat sources are applied at the vapor/wick interface for both the evaporator and condenser sections. These boundary conditions simulate the loss and gain of heat resulting from fluid evaporation and condensation, respectively. Depending on the direction of the vapor velocity, the term on the right-hand side changes sign to determine heat loss/gain per unit area.

c. Thermal Insulation

$$-\boldsymbol{n}\cdot\boldsymbol{q} = 0 \qquad (14)$$

Thermal insulation (no heat flux) is applied to all remaining external boundaries.

B. Vapor Flow

1. Governing Equations

$$\rho\frac{\delta \boldsymbol{u}}{\delta t} + \rho_v(\boldsymbol{u_v}\cdot\nabla)\boldsymbol{u_v} = -\nabla \mathrm{p_v} + \nabla\cdot(\mu_\mathrm{V}(\nabla\mathbf{u}_\mathrm{v} + (\nabla\mathbf{u}_\mathrm{v})^\mathrm{T}) - \frac{2}{3}\mu_\mathrm{v}(\nabla\cdot\mathbf{u}_\mathrm{v})\mathbf{I}) + \boldsymbol{F} + \rho_v\boldsymbol{g} \qquad (15)$$

$$\frac{\delta \rho}{\delta t} + \nabla\cdot(\rho_v\boldsymbol{u_v}) = 0 \qquad (16)$$

The Navier-Stokes equations are implemented to solve the laminar flow problem in the vapor chamber. The conservation of momentum is described with equation 15 and continuity is defined by equation 16. These equations are applied via the Laminar Flow module. Only the vapor domain is selected. Compressible flow is enabled, and gravity is included. Note: equation 3 accounts for heat transfer in the vapor flow regime.

2. Initial Conditions

$$\boldsymbol{u_v} = \mathbf{0} \qquad (17)$$

$$p_{0_v} = p_{sat}(T_0) + p_{hydro} \qquad (18)$$

$$p_{sat} = p_{ref}\cdot e^{\frac{h_{fg}M_n}{R*\left(\frac{1}{T_{ref}}-\frac{1}{T}\right)}} \qquad (19)$$

$$p_{hydro} = \rho_{ref}\boldsymbol{g}\cdot\left(\boldsymbol{r} - \boldsymbol{r}_{ref}\right) \qquad (20)$$

There is no initial vapor velocity at the start of the simulation (17). The initial pressure for the vapor domain is the sum of the saturation pressure at the initial temperature and hydrostatic pressure (18). Saturation pressure and hydrostatic pressure are defined in equations 19 and 20.

3. Boundary Conditions

a. Inlet

$$\boldsymbol{n}^T(-p_v\boldsymbol{I} + \mu_v(\nabla\boldsymbol{u}_v + (\nabla\boldsymbol{u}_v)^T) - \frac{2}{3}\mu_v(\nabla\cdot\boldsymbol{u}_v)\boldsymbol{I})\boldsymbol{n} = -(\hat{p}_{sat} + p_{hydro}) \qquad (21)$$

$$\boldsymbol{u} \cdot \boldsymbol{t} = 0 \quad (22)$$

A pressure condition is applied at the vapor/wick boundary in the evaporator section. Equation 21 represents a normal stress condition operating in tandem with a no-tangential stress condition [7]. This equation is supplemented with a tangential velocity condition (22) [7].

b. Outlet

$$(-p_v\boldsymbol{I} + \mu_v(\nabla \boldsymbol{u}_v + (\nabla \boldsymbol{u}_v)^T) - \tfrac{2}{3}\mu_v(\nabla \cdot \boldsymbol{u}_v)\boldsymbol{I})\boldsymbol{n} = -\left(\hat{p}_{sat} + p_{hydro}\right)\boldsymbol{n} \quad (23)$$

A similar pressure condition is also applied at the vapor/wick boundary in the condenser section.

c. Walls

$$\boldsymbol{u}_v = \boldsymbol{0} \quad (24)$$

A no slip condition is applied to all vapor chamber boundaries with the exception of the inlet and outlet.

C. Wick Flow

1. Governing Equations

$$\boldsymbol{u} = -\frac{K}{\mu_l}(\nabla p_l + \rho_l \boldsymbol{g}) \quad (25)$$

$$\frac{\delta}{\delta t}(\epsilon \rho_l) + \nabla \cdot (\rho_l \boldsymbol{u}) = Q_d \quad (26)$$

These equations are applied via the Darcy's Law module. Only the wick domain is selected. Gravitational effects are included. Equation 25 describes the general form of Darcy's law, which is a function of permeability, dynamic viscosity, pressure gradient, and gravity. Q_d in equation 26 represents discharge.

2. Initial Conditions

$$p_{0_w} = p_{ref} \cdot e^{\frac{h_{fg} M_n}{R^*\left(\frac{1}{T_{ref}} - \frac{1}{T_0}\right)}} \quad (27)$$

The initial pressure in the wick domain is equal to the saturation pressure at the initial temperature.

3. Boundary Conditions

a. Inlet and Outlet

$$p_{in_W} = p_{sat} \quad (28)$$

$$p_{out_w} = p_{sat} \quad (29)$$

The inlet equation is applied at the vapor/wick boundary in the evaporator section, and the outlet equation is applied at the vapor/wick boundary in the condenser section. Both boundary conditions are saturation pressure.

b. No Flow

$$-\boldsymbol{n} \cdot \rho_l \boldsymbol{u}_l = 0 \quad (30)$$

A no flow condition is applied to all boundaries for the wick other than the inlet and outlet.

II. Mesh Refinement Study – Validation of Mesh Independence

To verify that the construction of the finite element mesh was not influencing results, a mesh refinement study was performed. Two critical features for this model were used as tracking variables to determine mesh independence, thermal resistance and surface temperature. The parameters varied for the mesh refinement study were the maximum and minimum mesh element size, maximum element growth rate, and curvature factor. The values selected for these parameters are derived from the built-in, physics-based, and fluid dynamics optimized mesh building parameters: extra coarse, coarser, coarse, normal, fine, finer, and extra fine, respectively.

Table 3. Mesh Refinement Parameter Sweep

Parameter	Refinement Number						
Step number	1 (extra coarse)	2 (coarser)	3 (coarse)	4 (normal)	5 (fine)	6 (finer)	7 (extra fine)
Max mesh element size	0.39	0.261	0.201	0.135	0.105	0.084	0.039
Min mesh element size	0.015	0.012	0.009	0.006	0.003	0.0012	4.5E-4
Max element growth rate	1.3	1.25	1.2	1.15	1.13	1.1	1.08
Curvature factor	0.8	0.6	0.4	0.3	0.3	0.25	0.25

The maximum element growth rate refers to the maximum rate at which the size of an element can change from a region with small elements to a region with larger elements [7]. For example, if this parameter was set to 1.3, the element size could grow by a maximum of 30% from one element to the next. The curvature factor refers to the ratio between a boundary element's size, and the curvature radius of the boundary [7]. COMSOL internally multiples this curvature factor by the curvature radius to determine the mesh element size.

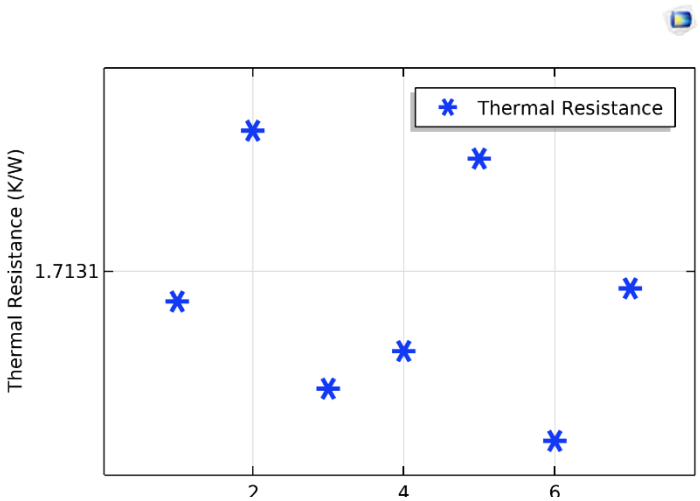

Figure 3. Thermal resistance for each mesh refinement step; 30W input, Lc = 20 mm, Le = 10 mm, $\theta = 90°$

The mesh refinement parametric sweep was performed with a heat input of 30 W, with a condenser length, L_c, of 20 mm, and an evaporator length, L_e, of 10 mm. The thermal resistance showed no appreciable differences until the 10th decimal place. This is far beyond the accuracy required for the purposes of this model. The surface temperature also showed no discernable differences between extra coarse and extra fine out to the 15th decimal place. These results indicate mesh insensitivity, and thus independence, for the mesh element sizes required for this simulation. Therefore, erring on the conservative side without imposing significant computational expense, refinement number 5 was selected.

III. Parametric Study Results

Parametric studies were performed for power input, condenser length, evaporator length and inclination. All but one parameter was held constant for each study. The subsequent effects on surface temperature, vapor/wick interface temperature, centerline temperature and pressure, and phase change heat flux, were studied and checked against existing literature for logical consistency in section A. Sections B through D are not substantiated against literature because there is no available trend data for the parametric sweeps that were performed. Testing in the laboratory with the LWHP prototypes is required to validate these results. Note: interface pressure is not included in these graphs as it is identical to the centerline pressure.

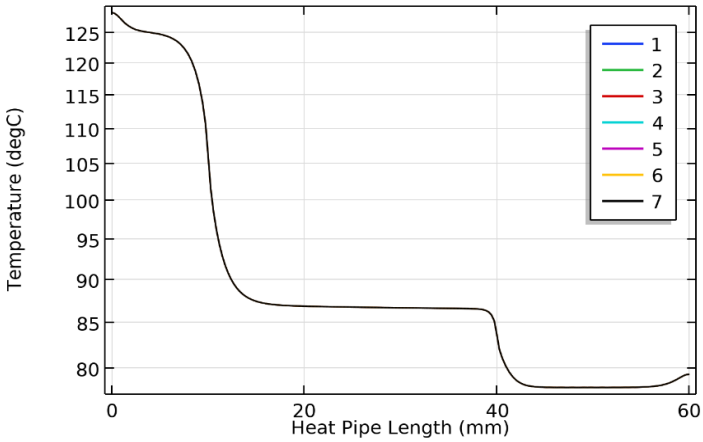

Figure 4. Surface temperature for each mesh refinement step; 30W input, Lc = 20 mm, Le = 10 mm, $\theta = 90°$.

All studies were performed with Inconel 718 as the wall/wick material, and water as the working fluid. The geometric configuration shown in Figure 5 matches the configuration of the existing lattice wick heat pipe prototypes.

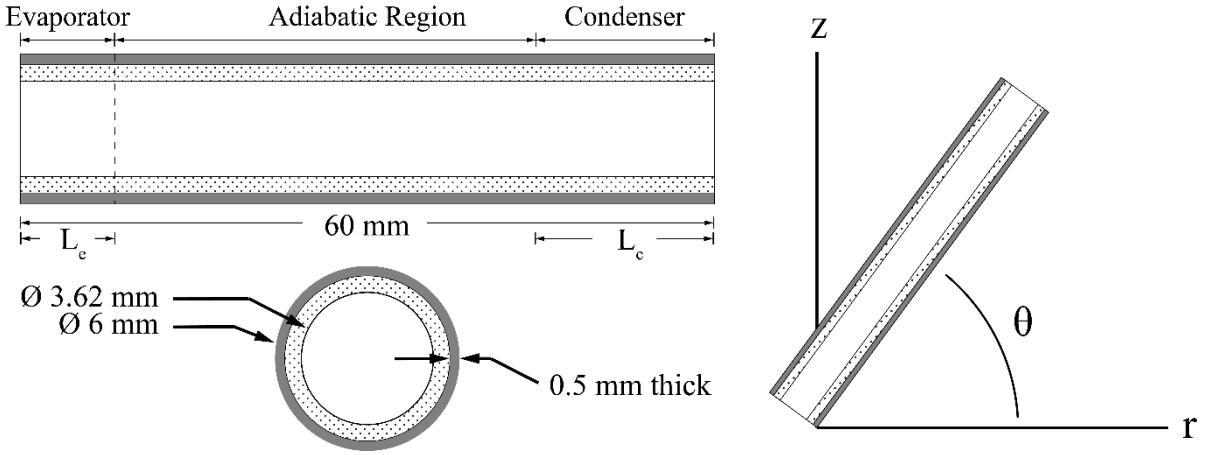

Figure 5. Geometric configuration used for parametric studies

A. Varying Heat Input & Conceptual Validation

The first study was performed by varying the heat input, Q_{in}. This parameter was swept from 10 W to 50 W, in increments of 10 W. L_c was held constant at 20 mm, and L_e at 10 mm. The heat pipe was oriented vertically ($\theta = 90°$) such that the evaporator was at the bottom, and gravity was pulling in the axial direction.

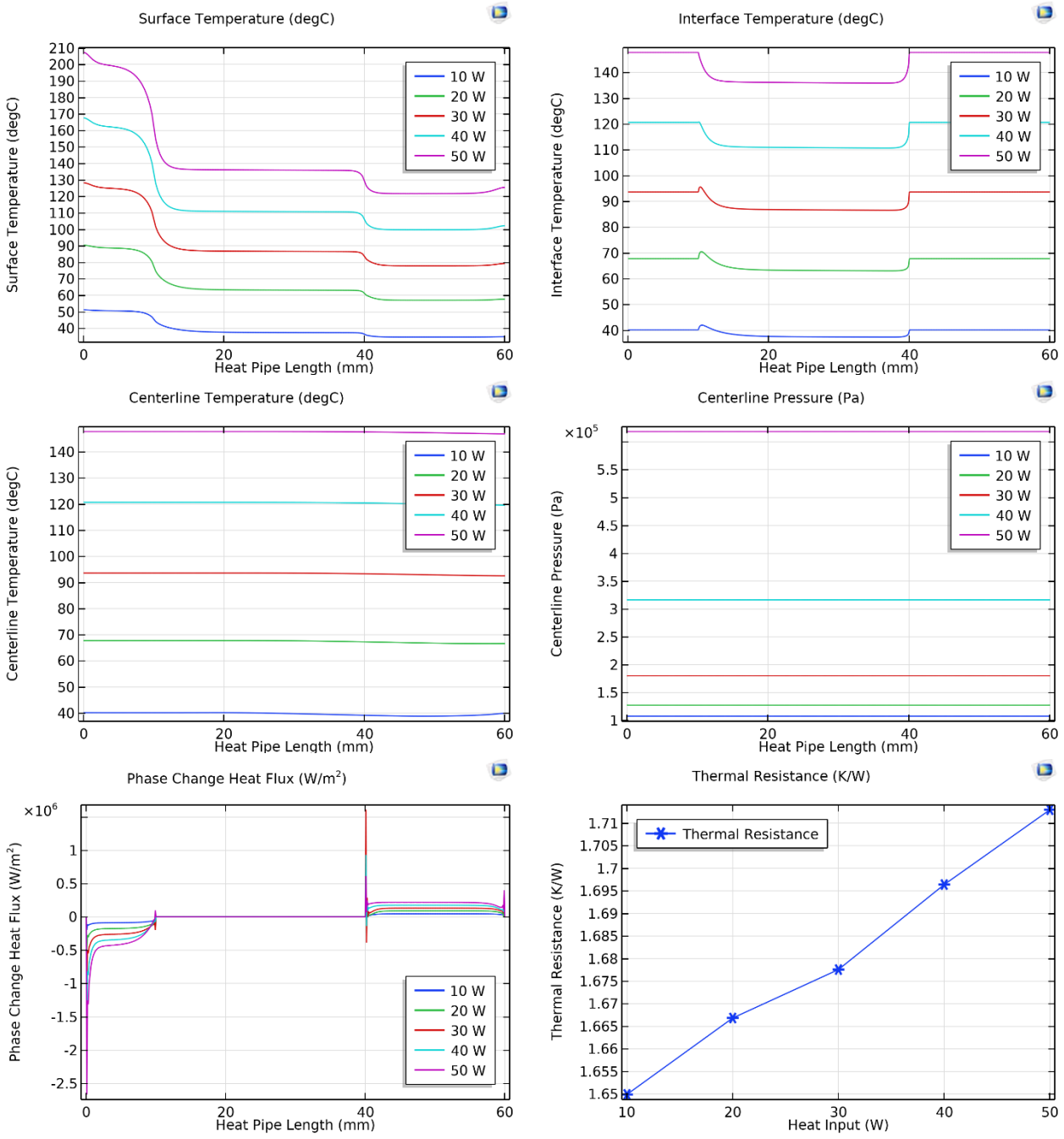

Figure 6. Results from 10 W to 50 W parametric heat input sweep; L_c = 20 mm, L_e = 10 mm, θ = 90°

The surface temperature qualitatively correlates with behavioral patterns seen in literature [9, 10, 11, 12]. As expected, the overall temperature increases with increasing heat input. The difference in temperature between condenser and evaporator sections increases with each iteration. This increase in overall temperature difference is likely a result of the trend seen in thermal resistance. As heat increases, thermal resistance increases. This behavior also matches patterns seen in literature [13].

The vapor/wick interface temperature is constant at the evaporator and condenser. This is consistent with the isothermal behavior observed during a phase change, indicating that the phase change heat flux term is acting as intended. Further supporting this conclusion is the presence of negative phase change heat flux terms in the evaporator, and positive terms in the condenser.

Centerline temperature and centerline pressure are very nearly constant. The vapor in heat pipes is expected to behave nearly isothermally, thus nearly isobaric, validating this result [1]. The magnitude of these values increases as heat input increases, which is logically consistent with the idea that at a constant volume, energy increase is directly proportional to temperature increase, which is directly proportional to pressure increase. Following this logic, all values present increasing magnitudes and spreads with increasing heat input.

B. Varying Condenser Length

The next study was performed by varying the condenser length, L_c. This parameter was swept from 10 mm to 30 mm, in increments of 5 mm. Q_{in} was held constant at 30 W, while L_e was held at 10 mm. The heat pipe was oriented vertically ($\theta = 90°$) such that the evaporator was at the bottom, and gravity was pulling in the axial direction.

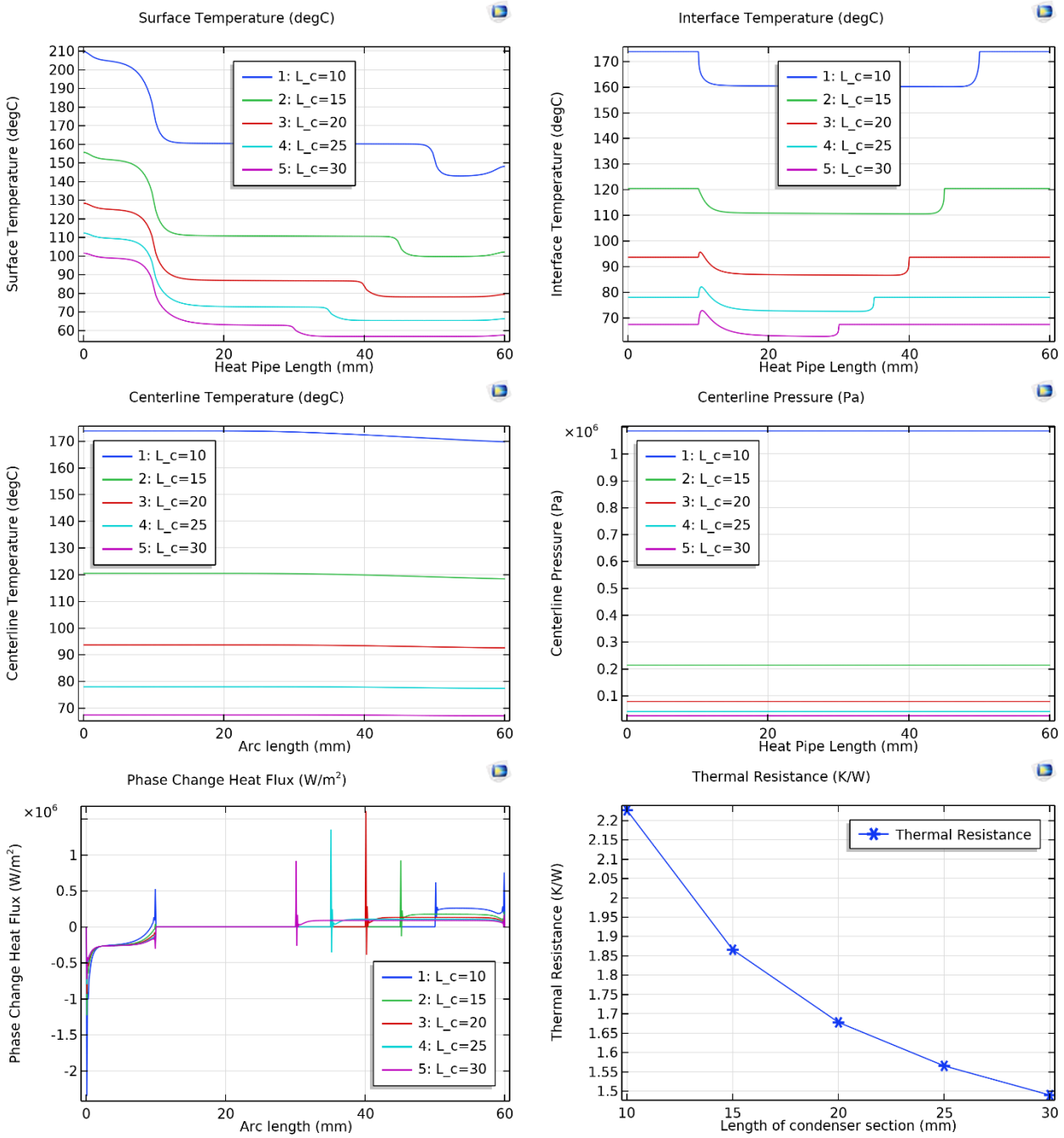

Figure 7. Results from 10 mm to 30 mm parametric condenser length sweep; Q_{in} = 30 W, L_e = 10 mm, θ = 90°

As the condenser length increases, the overall temperature of the heat pipe in both the surface and interface regions decreases. As seen in section A, varying heat input, constant vapor/wick interface inlet/outlet temperatures are maintained, and phase change heat flux follows the expected behaviors. A decrease in thermal resistance also makes physical sense as the calculation is based on the evaporator and condenser temperatures, which are both decreasing. Laboratory experimentation is required to determine the validity of these results.

C. Varying Evaporator Length

This study was performed by varying the evaporator length, L_e. This parameter was swept from 10 mm to 30 mm, in increments of 5 mm. Q_{in} was held constant at 30 W, while L_c was held at 10 mm. The heat pipe was oriented vertically ($\theta = 90°$) such that the evaporator was at the bottom, and gravity was pulling in the axial direction.

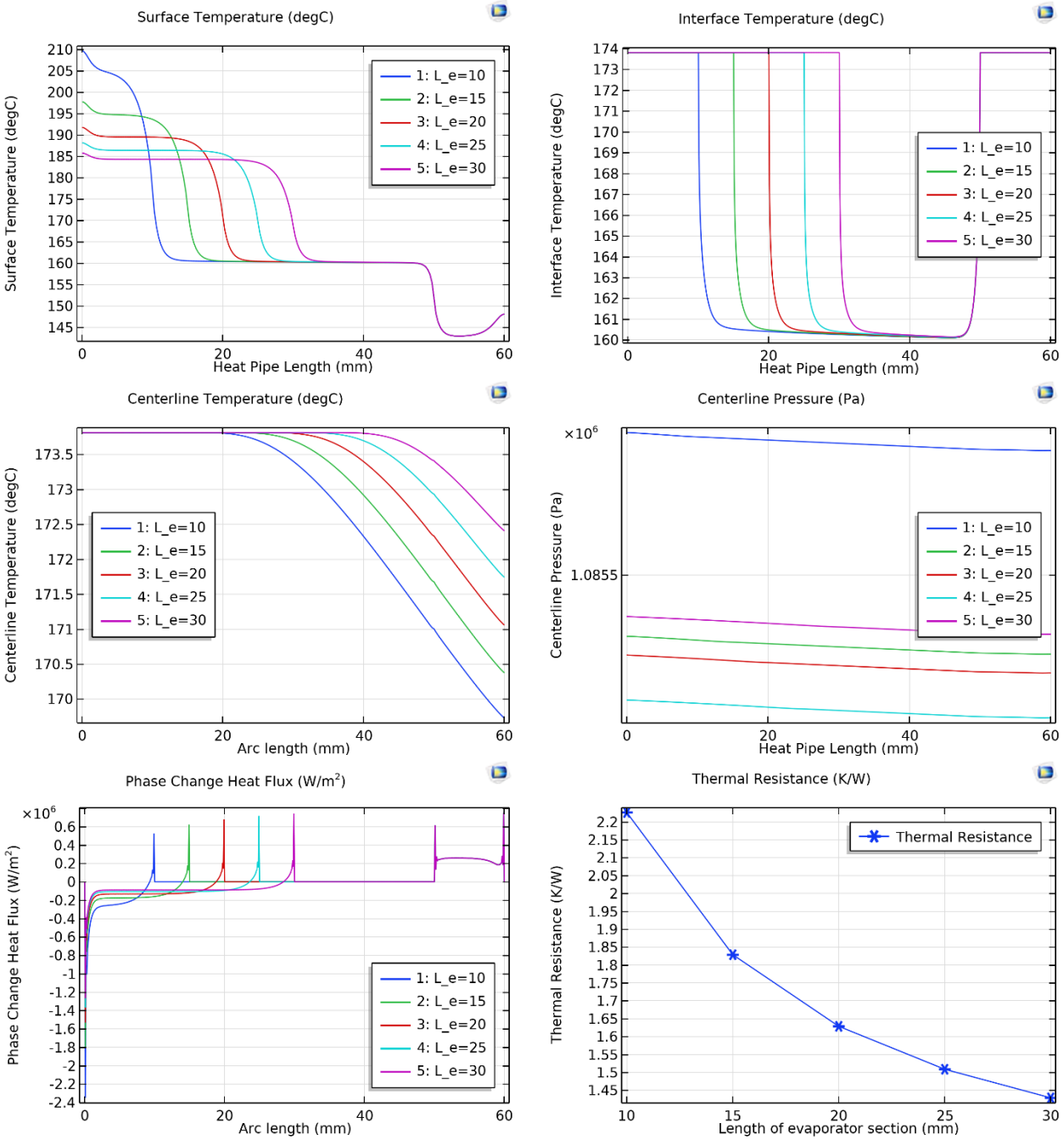

Figure 8. Results from 10 mm to 30 mm parametric evaporator length sweep; Q_{in} = 30 W, L_c = 10 mm, θ = 90°

The temperature trends here imply that, regardless of evaporator region length, the condenser temperature will remain constant. We also see a similar trend in the adiabatic and condenser sections in the vapor/wick interface. There is an increasing temperature and pressure fall-off along the centerline. The results for phase change heat flux and thermal resistance follow familiar behavioral trends to the results seen in section B. These results also require validation via physical experimentation.

D. Varying Inclination

The final study was performed by varying the inclination θ. Due to restrictions in how COMSOL defines 2D axially-symmetric geometries, a true rotation was not possible. Therefore, gravity was switched between pulling in the z-direction and pulling in the r-direction (with $\theta = 90°$) to simulate the rotation of the heat pipe. Q_{in} was held constant at 30 W, L_c was 20 mm, and L_e was 10 mm.

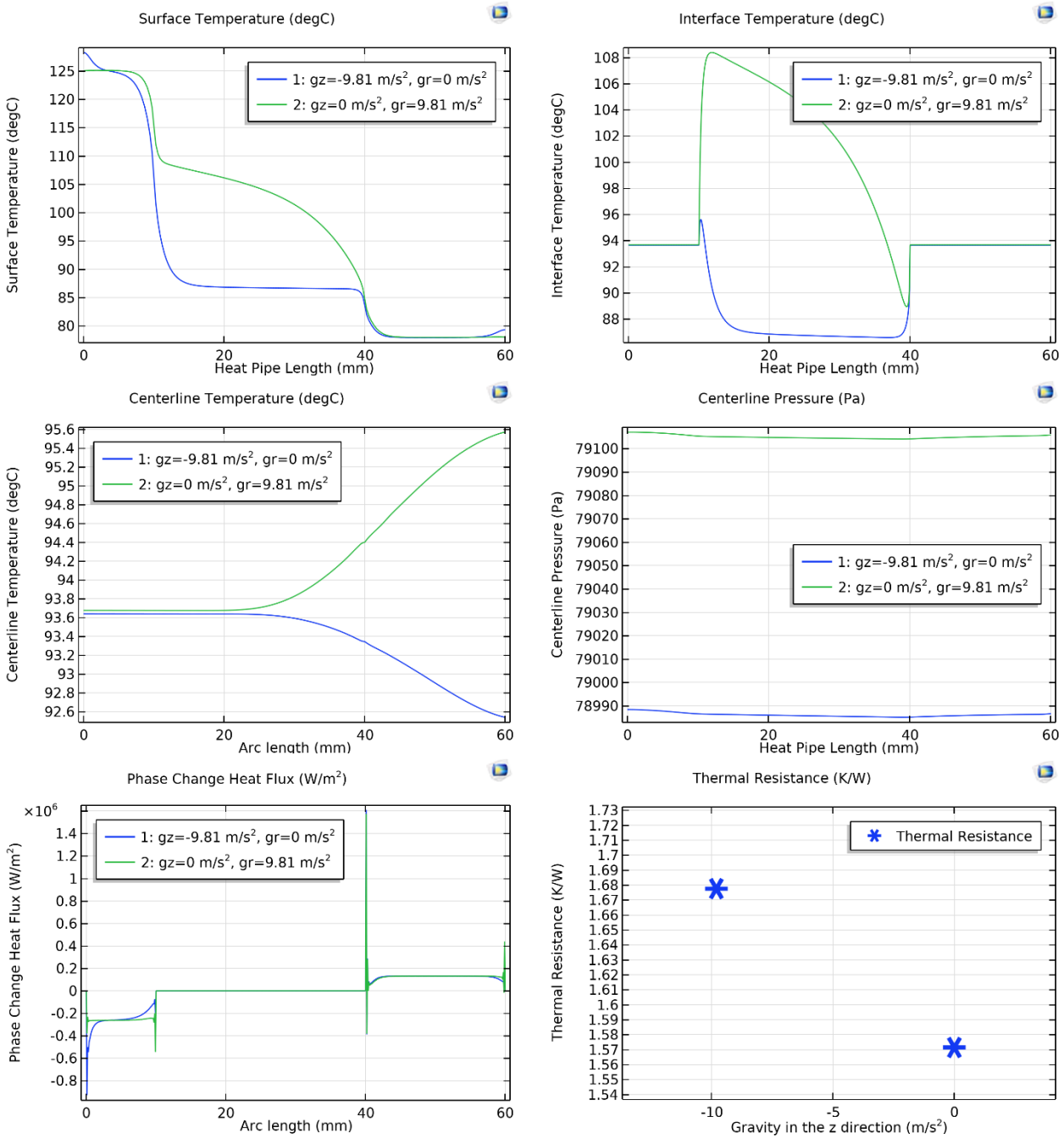

Figure 9. Results from inclination change; Q_{in} = 30 W, L_c = 20 mm, L_e = 10 mm

There is no available data in literature regarding how the behavior of lattice wick heat pipes will change with changes in orientation. Therefore, all the data shown here must be validated against laboratory experiments.

IV. Conclusion

In industry, it is common for manufacturers of heat pipes to rely on simple analytical equations to determine operational limits, then use these limits as a baseline for a design. As a design becomes more complex, for example using heat pipes to cool turbine vanes, these analytical equations become less and less valuable. Additive manufacturing makes complex implementations of heat pipes substantially more accessible, therefore the gap between what can be predicted by analytical equations alone and what will be required for the complex geometries of the future, is bound to get wider. A numerical model, such as the model presented here, is an effective way to bridge that growing gap. This model intends to provide a baseline configuration for the simplest lattice wick heat pipe, a cylinder, such that more sophisticated models can use the principles shown here to model their behaviors. This model is built in such a way that a designer could easily modify the heat pipe materials, working fluid, geometry, condenser length, evaporator length, heat input, heat rejection, and gravitational influences without much difficulty.

This model solves for steady state conditions, assuming laminar compressible gas flow in the vapor chamber and incompressible Newtonian flow in the wick section. Variants of the heat conduction transport equation in conjunction with Fourier's law are implemented to solve the conjugate heat transfer problem. An effective thermal conductivity is applied to the wick section to solve for the combined conductivity of the porous medium and fluid. Navier-Stokes equations are applied to the vapor flow, enforcing continuity and the conservation of momentum. The wick flow is described by Darcy's law, a method traditionally used in hydrology to measure fluid flow in sand or soil but applied here via the use of permeability and porosity values that match the prototype lattice wick. The general behaviors of the heat-pipe as analyzed during the heat input parametric sweep are in good qualitative agreement with results seen in literature. The results for the other parametric studies, however, require further investigation by means of laboratory experimentation to determine their validity.

Appendix

Term	**Temperature Dependent Equations for Steam** $(for\ 380.0K \leq T \leq 850.0K)$ [14]
$\mu_v =$	$-1.42022867E-6+(3.8345571E-8)T^1-(3.85222958E-12)T^2+(2.1019569E-15)T^3$
$C_{p_v} =$	$13604.7344-(90.4303506)T^1+(0.27735566)T^2-(4.21264496E-4)T^3$ $+(3.18369497E-7)T^4-(9.56147519E-11)T^5$
$\rho_v =$	$\frac{0.01802 \cdot p_{absolute}}{R \cdot T}$
$k_v =$	$1.31729321E-4+(5.14971428E-5)T^1+(3.89645315E-8)T^2-(1.36813161E-11)T^3$

Term	Temperature Dependent Equations for Water [14]
$\mu_l =$	$\underline{For\ 273.15K \leq T \leq 413.15K}$: $1.3799566804 - (0.021224019151)T^1 + (1.3604562827E-4)T^2 - (4.6454090319E-7)T^3 + (8.9042735735E-10)T^4 - (9.0790692686E-13)T^5 + (3.8457331488E-16)T^6$ $\underline{For\ 413.15K \leq T \leq 553.75K}$: $0.00401235783 - (2.10746715E-5)T^1 + (3.85772275E-8)T^2 - (2.39730284E-11)T^3$
$C_{p_l} =$	$\underline{For\ 273.15K \leq T \leq 553.75K}$: $12010.1471 - (80.4072879)T^1 + (0.309866854)T^2 - (5.38186884E-4)T^3 + (3.62536437E-7)T^4$
$\rho_l =$	$\underline{For\ 273.15K \leq T \leq 293.75K}$: $-950.704055329848 + (18.9229382407066)T - (0.060367639882855)T^2 + (0.000063092789034)T^3$ $\underline{For\ 293.15K \leq T \leq 373.75K}$: $432.257114008512 + (4.969288832655160)T - 0.013395065634452 * T^2 + (0.000010335053319)T^3$
$k_l =$	$\underline{For\ 273.15K \leq T \leq 553.75K}$: $-0.869083936 + 0.00894880345 * T^1 - 1.58366345E-5 * T^2 + 7.97543259E-9 * T^3$

Acknowledgments

A. M. Scott thanks Ezra McNichols for his excellent mentorship throughout this internship process. Thanks to Arman Mirhashemi, Doug Thurman, Paht Juangphanich, Paul Giel, and Phil Poinsette as well for their suggestions and guidance. Finally, thanks to Alexis Speer, Eric Hayes, and Monica Boyd, for their hard work ensuring a continued internship process during the challenging COVID-19 pandemic.

This research was funded by NASA's Internal Research and Development Program (IRAD), the Revolutionary Vertical Lift Technology (RVLT) project, and the Paragon TEC Internship program.

References

[1] Meseguer José, Pérez-Grasa Isabel, and Sanz-Andrés Angel, *Spacecraft thermal control*, Oxford: Woodhead Publishing, 2012, Chap. 11.

[2] Aerospace Specification Metals Inc, "Special Metals INCONEL® Alloy 718," *ASM Material Data Sheet* Available: http://asm.matweb.com/search/SpecificMaterial.asp?bassnum=NINC34.

[3] Jafari, D., Wits, W. W., and Geurts, B. J., "Metal 3D-printed wick structures for heat pipe application: Capillary performance analysis," *Applied Thermal Engineering* Available: https://www.sciencedirect.com/science/article/pii/S1359431118322981.

[4] Engineering Toolbox, "Heat Exchanger Heat Transfer Coefficients," *Engineering ToolBox* Available: https://www.engineeringtoolbox.com/heat-transfer-coefficients-exchangers-d_450.html.

[5] Cengel, Y., and Boles, M., "Thermodynamics: An Engineering Approach," *McGraw-Hill* Available: https://www.mheducation.com/highered/product/thermodynamics-engineering-approach-cengel-boles/M9781259822674.html.

[6] Prieto-Guerrero, A., and Espinosa-Paredes, G., "Propagation phenomena in boiling water reactors," *Linear and Non-Linear Stability Analysis in Boiling Water Reactors*, 2019, pp. 113–191.

[7] COMSOL, *COMSOL Multiphysics Reference Manual (For COMSOL 5.5)*, Stockholm, Sweden, 2019.

[8] Blazek, J., *Computational fluid dynamics principles and applications*, Oxford, UK: Elsevier, 2015, Chap. 2.

[9] A. Faghri., Analysis of frozen startup of high temperature heat pipes and three-dimensional modeling, Interim Report for Period January 1990–May 1991, Aero Propulsion and Power directorate, Wright Laboratory 1991.

[10] Pooyoo, N., Kumar, S., Charoensuk, J., and Suksangpanomrung, A., "Numerical simulation of cylindrical heat pipe considering non-Darcian transport for liquid flow inside wick and mass flow rate at liquid–vapor interface," *International Journal of Heat and Mass Transfer*, vol. 70, 2014, pp. 965–978.

[11] M. Shoeib., and M. Ali., "Numerical Simulation of a Conventional Heat Pipe," *International Journal of Mechanical, Aerospace, Industrial, Mechatronic and Manufacturing Engineering*, vol. 2, No 3, 2008.

[12] Hussain, M. N., Janajreh I., "Numerical Simulation of a Cylindrical Heat Pipe and Performance Study," *Int. J. of Thermal & Environmental Engineering*, vol 12, No 2, 2016, pp. 135-141

[13] De Ornelas, S., De Sousa, S., Dong, C., Fernelius, M., Hofer, M., Holsclaw, T., & Ninh, K. "Mathematical modeling, numerical simulation and statistical optimization of heat pipe design," 2006.

[14] Littmarck, S., Saeidi, F., *COMSOL Multiphysics 5.5*, Stockholm, Sweden, 2019.